Journal of Sound and Vibration (2001) **245**(5), 785–800
doi:10.1006/jsvi.2001.3614, available online at http://www.idealibrary.com on IDEAL®

THE MODELLING AND VIBRATION CONTROL OF BEAMS WITH ACTIVE CONSTRAINED LAYER DAMPING

Y. M. Shi, Z. F. Li, H. X. Hua and Z. F. Fu

The National Key Laboratory for Vibration, Shock & Noise, Shanghai Jiaotong University, 200030 *Shanghai, People's Republic of China. E-mail: shiyinming@sina.com*

AND

T. X. Liu

The School of Mechanical Engineering, Shanghai Jiaotong University, 200030 *Shanghai, People's Republic of China*

(*Received* 12 *July* 2000, *and in final form* 8 *December* 2000)

The finite element method (FEM) is combined with the Golla–Hughes–McTavish (GHM) model of viscoelastic materials (VEM) to model a cantilever beam with active constrained layer damping treatments. This approach avoids time-consuming iteration in solving modal frequencies, modal damping ratios and responses. But the resultant finite element (FE) model has too many degrees of freedom (d.o.f.s) from the point of view of control, nor is it observable and controllable. A new model reduction procedure is proposed. An iterative dynamic condensation is performed in the physical space, and Guyan condensation is taken as an initial iteration approximation. A reduced order model (ROM) of suitable size emerges, but it is still not observable and controllable. Accordingly, a robust model reduction method is then employed in the state space. A numerical example proves that this procedure reduces the model and assures the stability, controllability and observability of the final reduced order model (FROM). Finally, a controller is designed by linear-quadratic Gaussian (LQG) method based on the FROM. The vibration attenuation is evident.

1. INTRODUCTION

Conventional passive constrained layer damping (PCLD) treatments [1–3] have been applied to machines and structures widely over the last century because of their reliability and simplicity, but they are not intelligent. Once the damping treatments are installed, they cannot be adjusted and cannot adapt to changeable environments. Recently, active damping has received increased attention in the aeronautic and astronautic industries, owing to the significant and adjustable damping traditional PCLD treatments cannot provide. Yet, in spite of productive research into active damping treatments [4–6], limitations remain. Safety and reliability cannot be guaranteed, and active damping is difficult to implement at high frequency ranges. To obtain hybrid damping, active constrained layer damping (ACLD) treatments [7, 8] have been proposed for replacing the constraining layer of PCLD treatments by a piezoelectric (PZT) layer.

Dynamic analysis and vibration control design require a reasonable mathematical model. FEM combined with GHM [9, 10] model of VEM is the popular method for modelling ACLD treatments. This combination is used in this paper to model a cantilever beam with ACLD treatments. It avoids time-consuming iteration for solving modal frequencies, modal

0022-460X/01/350785 + 16 $35.00/0

damping ratios and responses. But in terms of control, the FE model has too many degrees of freedom (d.o.f.s). A new model reduction procedure is proposed. An iterative dynamic condensation is performed in the physical space, and Guyan condensation is taken as an initial iteration approximation. A ROM of appropriate size emerges, but it is still not observable and controllable. A robust model reduction method in the state space follows. A numerical example proves that this procedure reduces the system and guarantees the FROM stability, controllability and observability. Finally, a controller based on the FROM is designed by LQG method. Vibration attenuation is evident.

2. FINITE ELEMENT MODEL

Figure 1 is a cantilever beam with partially covered ACLD. An FE model is developed based on the following assumptions: (1) The rotary inertia is negligible. Shear deformations in the PZT and the base beam are negligible. (2) The transverse displacement w is the same for all three layers. (3) Young's modulus of the VEM is negligible compared to those of the beam and PZT materials. (4) Linear theories of elasticity, viscoelasticity, and piezoelectricity are used. (5) There is perfect continuity at the interface, and no slip occurs between the layers. (6) The applied voltage is uniform along the beam. (7) Density and thickness are uniform over the beam.

The model for the cantilever beam with partially covered ACLD is divided into ACLD elements and plain beam elements.

2.1. ACLD ELEMENTS

Figure 2 shows an ACLD element. Nodal displacements are given by

$$\{U^{(e)}\} = \{w_i^{(e)}\ \theta_i^{(e)}\ u_{ci}^{(e)}\ u_{bi}^{(e)}\ w_j^{(e)}\ \theta_j^{(e)}\ u_{cj}^{(e)}\ u_{bj}^{(e)}]^{\mathrm{T}}. \tag{1}$$

The transverse displacement, the axial displacement of base beam and the axial displacement of PZT are expressed in the nodal displacements by finite element shape functions

$$w = [N_w]\{U^{(e)}\}, \quad \theta = [N_w]'\{U^{(e)}\}, \quad u_c = [N_c]\{U^{(e)}\}, \quad u_b = [N_b]\{U^{(e)}\}, \tag{2}$$

where the shape functions are given by

$$[N_w] = [1 - 3\xi^2 + 2\xi^3\ (\xi - 2\xi^2 + \xi^3)L_e\ 0\ 0\ 3\xi^2 - 2\xi^3\ (-\xi^2 + \xi^3)L_e\ 0\ 0],$$

$$[N_c] = [0\ 0\ 1 - \xi\ 0\ 0\ 0\ \xi\ 0], \quad [N_b] = [0\ 0\ 0\ 1 - \xi\ 0\ 0\ 0\ \xi], \tag{3}$$

where $\xi = x/L_e$.

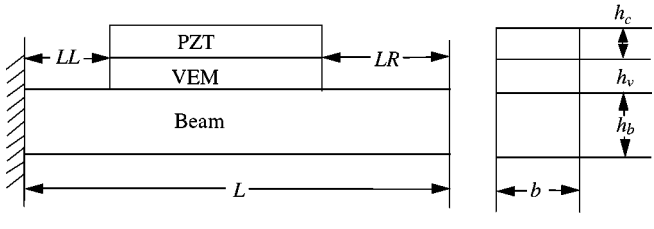

Figure 1. Cantilever beam with partially covered ACLD.

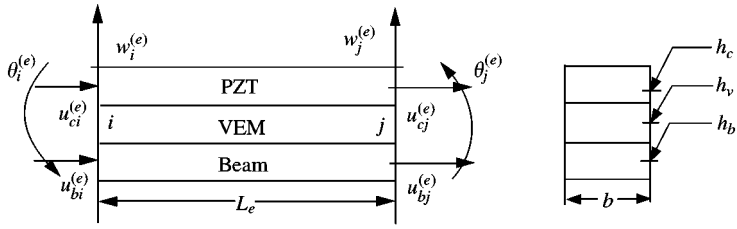

Figure 2. An ACLD element.

From the kinematic relationships between PZT layer and the base beam, it is easy to derive the following relation [11]:

$$u_v = \frac{u_c + u_b}{2} + \frac{(h_c - h_b)}{4}\frac{\partial w}{\partial x},$$

$$\gamma = \frac{u_c - u_b}{h_v} + \frac{\partial w}{\partial x}\left(\frac{h_c + h_b + 2h_v}{2h_v}\right) \tag{4}$$

γ and u_v can be expressed in the nodal displacement as follows:

$$u_v = [N_v]\{U^{(e)}\}, \quad \gamma = [N_\gamma]\{U^{(e)}\}, \tag{5}$$

where

$$[N_v] = \frac{1}{2}([N_c] + [N_b]) + \frac{h_c - h_b}{4}[N_w]',$$

$$[N_\gamma] = \frac{1}{h_v}\left[-\frac{6h^*}{L_e}\xi + \frac{6h^*}{L_e}\xi^2 \; h^*(1 - 4\xi + 3\xi^2) \; 1 - \xi \; \xi - 1 \right.$$

$$\left. \frac{6h^*}{L_e}\xi - \frac{6h^*}{L_e}\xi^2 \; h^*(-2\xi + 3\xi^2) \; \xi \; -\xi\right],$$

$$h^* = (h_c - h_b)/4.$$

2.1.1. *Base beam layer*

The potential energy of beam due to axial displacements is

$$\frac{1}{2}\int_0^{L_e} E_b b h_b \left(\frac{\partial u_b}{\partial x}\right)^2 \mathrm{d}x = \frac{1}{2}\{U^{(e)}\}^{\mathrm{T}}[K_{bu}^{(e)}]\{U^{(e)}\}, \quad [K_{bu}^{(e)}] = E_b b h_b L_e \int_0^1 [N_b]'^{\mathrm{T}}[N_b]' \,\mathrm{d}\xi. \tag{6}$$

The potential energy of beam due to transverse displacements is

$$\frac{1}{2}\int_0^{L_e} E_b I_b \left(\frac{\partial^2 w}{\partial x^2}\right)^2 \mathrm{d}x = \frac{1}{2}\{U^{(e)}\}^{\mathrm{T}}[K_{bw}^{(e)}]\{U^{(e)}\}, \quad [K_{bw}^{(e)}] = E_b I_b L_e \int_0^1 [N_w]''^{\mathrm{T}}[N_w]'' \,\mathrm{d}\xi. \tag{7}$$

The kinetic energy of beam due to axial displacements is

$$\frac{1}{2}\int_0^{L_e}\rho_b h_b b\left(\frac{\partial u_b}{\partial t}\right)^2 \mathrm{d}x = \frac{1}{2}\{\dot{U}^{(e)}\}^{\mathrm{T}}[M_{bu}^{(e)}]\{\dot{U}^{(e)}\}, \quad [M_{bu}^{(e)}] = \rho_b h_b b L_e \int_0^1 [N_b]^{\mathrm{T}}[N_b]\,\mathrm{d}\xi. \tag{8}$$

The kinetic energy of beam due to transverse displacements is

$$\frac{1}{2}\int_0^{L_e}\rho_b h_b b\left(\frac{\partial w}{\partial t}\right)^2 \mathrm{d}x = \frac{1}{2}\{\dot{U}^{(e)}\}^{\mathrm{T}}[M_{bw}^{(e)}]\{\dot{U}^{(e)}\}, \quad [M_{bw}^{(e)}] = \rho_b h_b b L_e \int_0^1 [N_w]^{\mathrm{T}}[N_w]\,\mathrm{d}\xi. \tag{9}$$

2.1.2. *PZT Layer*

For one-dimensional structures with uni-axial loading, the constitutive equations of PZT materials can be written as

$$\begin{bmatrix}\varepsilon\\ D\end{bmatrix} = \begin{bmatrix}S_{11}^E & d_{31}\\ d_{31} & \varepsilon_{33}^{\tau}\end{bmatrix}\begin{bmatrix}\tau\\ E\end{bmatrix}. \tag{10}$$

From equation (10), the potential energy of PZT layer due to axial displacements is

$$\frac{1}{2}\int_0^{L_e} E_c b h_c\left(\frac{\partial u_c}{\partial x}\right)^2 \mathrm{d}x = \frac{1}{2}\{U^{(e)}\}^{\mathrm{T}}[K_{cu}^{(e)}]\{U^{(e)}\}, \quad [K_{cu}^{(e)}] = E_c b h_c L_e \int_0^1 [N_c]'^{\mathrm{T}}[N_c]'\,\mathrm{d}\xi. \tag{11}$$

The potential energy of PZT layer due to transverse displacements is

$$\frac{1}{2}\int_0^{L_e} E_c I_c\left(\frac{\partial^2 w}{\partial x^2}\right)^2 \mathrm{d}x = \frac{1}{2}\{U^{(e)}\}^{\mathrm{T}}[K_{cw}^{(e)}]\{U^{(e)}\}, \quad [K_{cw}^{(e)}] = E_c I_c L_e \int_0^1 [N_w]''^{\mathrm{T}}[N_w]''\,\mathrm{d}\xi. \tag{12}$$

The kinetic energy of PZT layer due to axial displacements is

$$\frac{1}{2}\int_0^{L_e}\rho_c h_c b\left(\frac{\partial u_c}{\partial t}\right)^2 \mathrm{d}x = \frac{1}{2}\{\dot{U}^{(e)}\}^{\mathrm{T}}[M_{cu}^{(e)}]\{\dot{U}^{(e)}\}, \quad [M_{cu}^{(e)}] = \rho_c h_c b L_e \int_0^1 [N_c]^{\mathrm{T}}[N_c]\,\mathrm{d}\xi. \tag{13}$$

The kinetic energy of PZT layer due to transverse displacements is

$$\frac{1}{2}\int_0^{L_e}\rho_c h_c b\left(\frac{\partial w}{\partial t}\right)^2 \mathrm{d}x = \frac{1}{2}\{\dot{U}^{(e)}\}^{\mathrm{T}}[M_{cw}^{(e)}]\{\dot{U}^{(e)}\}, \quad [M_{cw}^{(e)}] = \rho_c h_c b L_e \int_0^1 [N_w]^{\mathrm{T}}[N_w]\,\mathrm{d}\xi. \tag{14}$$

The virtual work done by the induced strain (force) is

$$\delta w_c = \int_0^{L_e} E_c d_{31} b v(t)\delta\left(\frac{\partial u_c}{\partial x}\right)\mathrm{d}x = [\delta U^{(e)}]^{\mathrm{T}}\{f_c^{(e)}\}, \tag{15}$$

where $\{f_c^{(e)}\} = E_c d_{31} b v(t)[0\ 0\ -1\ 0\ 0\ 0\ 1\ 0]^{\mathrm{T}}$.

2.1.3. *VEM layer*

For one-dimensional structures, the GHM model represents the shear modulus of VEM as a series of mini-oscillator terms in the Laplace domain [9, 10]

$$s\tilde{G}(s) = G^{\infty}\left[1 + \sum_{k=1}^{N} \alpha_k \frac{s^2 + 2\hat{\zeta}_k\hat{\omega}_k s}{s^2 + 2\hat{\zeta}_k\hat{\omega}_k s + \hat{\omega}_k^2}\right]. \tag{16}$$

The positive constants $\alpha_k, \hat{\omega}_k, \hat{\zeta}_k$ govern the shape of the modulus function over the complex s-domain.

The potential energy of VEM layer due to the shear strain can be written as follows:

$$\frac{1}{2}\int_0^{L_e} G_v b h_v \gamma^2 \,\mathrm{d}x = \frac{1}{2}\{U^{(e)}\}^{\mathrm{T}}[K_{v\gamma}^{(e)}]\{U^{(e)}\}, \quad [K_{v\gamma}^{(e)}] = G_v b h_v L \int_0^1 [N_\gamma]^{\mathrm{T}}[N_\gamma]\,\mathrm{d}\xi. \tag{17}$$

The kinetic energy of VEM layer due to axial displacements is

$$\frac{1}{2}\int_0^{L_e} \rho_v h_v b \left(\frac{\partial u_v}{\partial t}\right)^2 \mathrm{d}x = \frac{1}{2}\{\dot{U}^{(e)}\}^{\mathrm{T}}[M_{vu}^{(e)}]\{\dot{U}^{(e)}\}, \quad [M_{vu}^{(e)}] = \rho_v h_v b L_e \int_0^1 [N_v]^{\mathrm{T}}[N_v]\,\mathrm{d}\xi. \tag{18}$$

The kinetic energy of VEM layer due to transverse displacements is

$$\frac{1}{2}\int_0^{L_e} \rho_v h_v b \left(\frac{\partial w}{\partial t}\right)^2 \mathrm{d}x = \frac{1}{2}\{\dot{U}^{(e)}\}^{\mathrm{T}}[M_{vw}^{(e)}]\{\dot{U}^{(e)}\}, \quad [M_{vw}^{(e)}] = \rho_v h_v b L_e \int_0^1 [N_w]^{\mathrm{T}}[N_w]\,\mathrm{d}\xi. \tag{19}$$

2.2. PLAIN BEAM ELEMENTS

The stiffness and mass matrices of plain beam elements have dimensions of 6×6. They are similar to equations (6)–(9).

2.3. LOAD VECTOR

The virtual work done by external disturbance force is

$$\delta w_d = \int_0^{L_e} f_d(x, t)\delta w(x, t)\,\mathrm{d}x = [\delta U^{(e)}]^{\mathrm{T}}\{f_d\}. \tag{20}$$

It is usually more convenient to consider the effects of such force at the global level.

2.4. THE DYNAMIC EQUATION OF CANTILEVER BEAM WITH ACLD TREATMENTS

For the ACLD elements, the element equations can be written as

$$[M^{(e)}]\{\ddot{U}^{(e)}\} + [K_E^{(e)}]\{U^{(e)}\} + [K_{v\gamma}^{(e)}]\{U^{(e)}\} = \{f_c^{(e)}\},$$

where

$$[M^{(e)}] = [M_{bu}^{(e)}] + [M_{bw}^{(e)}] + [M_{cu}^{(e)}] + [M_{cw}^{(e)}] + [M_{vu}^{(e)}] + [M_{vw}^{(e)}],$$

$$[K_E^{(e)}] = [K_{bu}^{(e)}] + [K_{bw}^{(e)}] + [K_{cu}^{(e)}] + [K_{cw}^{(e)}]. \tag{21}$$

Equation (21) is a non-linear equation because G_v in $[K_{v\gamma}^{(e)}]$ is not a constant. In Laplace domain the initial conditions have been assumed to be zero, so a column matrix of dissipation co-ordinates is introduced

$$\{\hat{Z}_k(s)\} = \frac{\hat{\omega}_k^2}{s^2 + 2\hat{\xi}_k\hat{\omega}_k s + \hat{\omega}_k^2}\{U^{(e)}(s)\}. \tag{22}$$

From the GHM model of VEM, equation (21) can be written as follows:

$$[\bar{M}^{(e)}]\{\ddot{q}^{(e)}\} + [\bar{D}^{(e)}]\{\dot{q}^{(e)}\} + [\bar{K}^{(e)}]\{q^{(e)}\} = \{\bar{f}^{(e)}\}, \tag{23}$$

$$\bar{M}^{(e)} = \begin{bmatrix} M^{(e)} & 0 & \cdots & 0 \\ 0 & \alpha_1 \dfrac{1}{\hat{\omega}_1^2}\Lambda & 0 & \vdots \\ \vdots & 0 & \ddots & 0 \\ 0 & \cdots & 0 & \alpha_N \dfrac{1}{\hat{\omega}_N^2}\Lambda \end{bmatrix}, \quad \bar{D}^{(e)} = \begin{bmatrix} 0 & 0 & \cdots & 0 \\ 0 & \alpha_1 \dfrac{2\hat{\xi}_1}{\hat{\omega}_1}\Lambda & 0 & \vdots \\ \vdots & 0 & \ddots & 0 \\ 0 & \cdots & 0 & \alpha_N \dfrac{2\hat{\xi}_N}{\hat{\omega}_N}\Lambda \end{bmatrix},$$

$$\bar{K}^{(e)} = \begin{bmatrix} K_E^{(e)} + K_{v\gamma}^{(e)}(1 + \sum_{k=1}^{N}\alpha_k) & -\alpha_1 R & \cdots & -\alpha_N R \\ -\alpha_1 R^{\mathrm{T}} & \alpha_1\Lambda & 0 & 0 \\ \vdots & 0 & \ddots & 0 \\ -\alpha_N R^{\mathrm{T}} & 0 & 0 & \alpha_N\Lambda \end{bmatrix},$$

$$\{q^{(e)}\} = \begin{Bmatrix} U^{(e)} \\ Z_1 \\ \vdots \\ Z_N \end{Bmatrix}, \quad \{\bar{f}^{(e)}\} = \begin{Bmatrix} f_c^{(e)} \\ 0 \\ \vdots \\ 0 \end{Bmatrix},$$

where $Z_k = R_v^{\mathrm{T}}\hat{Z}_k$, $R = R_v\Lambda$, $\Lambda = G^{\infty}\Lambda_v$, $[K_{v\gamma}^{(e)}] = G^{\infty}[\hat{K}_{v\gamma}^{(e)}]$, $[\hat{K}_{v\gamma}^{(e)}] = R_v\Lambda_v R_v^{\mathrm{T}}$, Λ_v is a diagonal matrix of the non-zero (necessarily positive) eigenvalues of matrix $\hat{K}_{v\gamma}^{(e)}$, the corresponding orthonormalized eigenvectors form the columns of the matrix R_v.

It is obvious that equation (23) is in the traditional second order form. For the cantilever beam with ACLD treatments, the following global dynamic equation can be derived through standard FEM assembling procedures:

$$[M]\{\ddot{q}\} + [D]\{\dot{q}\} + [K]\{q\} = [F]. \tag{24}$$

3. THE MODEL REDUCTION PROCESS

The dynamic equation (24) derived by FEM has an excess of d.o.f.s from a control point of view. Moreover, it is unobservable and uncontrollable [12, 13]. Model reduction is required.

Model reduction methods are developed from two different disciplines [14]: the FEM analysis [15, 16] and the large-system control theories [12, 17]. The former could reduce system size, but it could not guarantee observability and controllability because the model reduction takes place entirely in the physical space. Observability and controllability are beyond consideration. The latter could guarantee observability and controllability, but it is unsuitable for flexile structures like the ACLD system. The FE model of the ACLD system has too many d.o.f.s for adequate control, especially after the introduction of dissipation co-ordinates in equations (22) and (23). What is more, this large system is uncontrollable and unobservable. It is impossible to compute directly the full orthogonal bases for eigenspace required in intermediate steps in state space, even by Schur decomposition.

A new model reduction procedure is proposed. An iterative dynamic condensation is performed in the physical space, and Guyan condensation is taken as an initial iteration approximation. This results in a reduced order system of suitable size, but it is unobservable and uncontrollable. A robust model reduction method is employed in the state space afterwards. System size is reduced, and stability, controllability and observability of FROM are assured.

To study observability and controllability of the proposed model reduction procedure conveniently, controllability gramian W_c and the observability gramian W_o are introduced.

Given the continuous-time state-space model

$$\dot{x} = Ax + Bu, \qquad y = Cx + Du \tag{25}$$

W_c and W_o are defined by

$$W_c = \int_0^\infty \mathrm{e}^{A\tau} B B^{\mathrm{T}} \mathrm{e}^{A^{\mathrm{T}}\tau}\,\mathrm{d}\tau, \quad W_o = \int_0^\infty \mathrm{e}^{A^{\mathrm{T}}\tau} C^{\mathrm{T}} C \mathrm{e}^{A\tau}\,\mathrm{d}\tau. \tag{26}$$

W_c and W_o can be obtained by solving the Lyapunov equations

$$AW_c + W_c A^{\mathrm{T}} + BB^{\mathrm{T}} = 0, \quad A^{\mathrm{T}} W_o + W_o A + C^{\mathrm{T}} C = 0. \tag{27}$$

The system is controllable if W_c is full rank; it is observable if W_o is full rank [14]. The condition of W_c and W_o is a measure of the system's controllability and its observability.

3.1. THE MODEL REDUCTION IN THE PHYSICAL SPACE

The total d.o.f.s of equation (24) is assumed to be n. It can be divided into master d.o.f.s (the conserved d.o.f.s) and slave d.o.f.s (the removed d.o.f.s). Equation (24) can be written as

$$\begin{bmatrix} M_{mm} & M_{ms} \\ M_{sm} & M_{ss} \end{bmatrix} \begin{Bmatrix} \ddot{X}_m(t) \\ \ddot{X}_s(t) \end{Bmatrix} + \begin{bmatrix} D_{mm} & D_{ms} \\ D_{sm} & D_{ss} \end{bmatrix} \begin{Bmatrix} \dot{X}_m(t) \\ \dot{X}_s(t) \end{Bmatrix} + \begin{bmatrix} K_{mm} & K_{ms} \\ K_{sm} & K_{ss} \end{bmatrix} \begin{Bmatrix} X_m(t) \\ X_s(t) \end{Bmatrix} = \begin{bmatrix} F_m(t) \\ F_s(t) \end{bmatrix}. \tag{28}$$

Define system reduction matrix $R \in R^{s \times m}$, which relates the master d.o.f.s with the slave d.o.f.s, then after i iterations, the reduced order system equation [18] is

$$M_R^{(i)} \ddot{X}_m(t) + D_R^{(i)} \dot{X}_m(t) + K_R^{(i)} X_m(t) = F_R^{(i)}(t), \tag{29}$$

where

$$M_R^{(i)} = M_{mm} + (R^{(i)})^{\mathrm{T}} M_{sm} + M_{ms} R^{(i)} + (R^{(i)})^{\mathrm{T}} M_{ss} R^{(i)},$$

$$D_R^{(i)} = D_{mm} + (R^{(i)})^{\mathrm{T}} D_{sm} + D_{ms} R^{(i)} + (R^{(i)})^{\mathrm{T}} D_{ss} R^{(i)},$$

$$K_R^{(i)} = K_{mm} + (R^{(i)})^{\mathrm{T}} K_{sm} + K_{ms} R^{(i)} + (R^{(i)})^{\mathrm{T}} K_{ss} R^{(i)}, \quad F_R^{(i)}(t) = F_m(t) + (R^{(i)})^{\mathrm{T}} F_s,$$

$$R^{(i+1)} = -K_{ss}^{-1} [M_{ss} R^{(i)} (M_R^{(i)})^{-1} K_R^{(i)} - K_{sm}].$$

Guyan [15] condensation is taken as an initial iteration approximation. So $R^{(0)} = -K_{ss}^{-1} K_{sm}$.

In this reduction, two issues must be addressed: selection of the master d.o.f.s, and their number. Levy [19] gave guidance on choosing master d.o.f.s. He recommended the choice of d.o.f.s with large displacements in the useful band or large mass components. Ramsden and Stocker [20] selected the master d.o.f.s associated with large mass concentrations and those reasonably flexible with respect to other mass concentrations. Downs [21] insisted that master d.o.f.s must be translations instead of rotations. In complicated assemblies, master d.o.f.s were to be found in the most flexible regions. Shah and Raymund [22] proposed an eliminated algorithm, such that the ratio k_{ii}/m_{ii} of the diagonal terms of K and M corresponding to the removed slave d.o.f.s is a maximum. The number of interested modals determines the number of master d.o.f.s. Levy [19] advised that the ratio between the number of master d.o.f.s and the number of interested modals should be 3·5. Ramsden and Stocker [20] thought that the ratio should have a value between 2 and 3. Suarez [23] proposed a 1·40 ratio. Those conflicting theories make it difficult to resolve the issue of master d.o.f.s selection and their number. Different problems will require different solutions.

3.2. THE MODEL REDUCTION IN THE STATE SPACE

The reduced order system equation (29) is much smaller than the original system equation (24), but it is unobservable and uncontrollable in the state space. A robust model reduction follows in the state space. Generally speaking, the robust model reduction method has the following special features: (1) It bypasses the ill-conditioned balanced transformation. (2) It employs Schur decomposition to compute robustly the orthogonal bases for eigenspace required in intermediate steps. (3) It has an H^{∞}-norm error bound. The infinity norm of the relative error or the absolute error of the reduced order model is bounded by a precomputable positive real number for all frequencies.

Equation (29) can be transformed into the state-space form (A, B, C, D), with $2m$ d.o.f.s. Its transfer function is $G(s) = D + C(Is - A)^{-1}$. It can be reduced to a system with $k (k < 2m)$ d.o.f.s. The detailed procedure [12] is as follows:

(1) Solve matrices P and Q from the following Lyapunov equations:

$$PA^{\mathrm{T}} + AP + BB^{\mathrm{T}} = 0, \quad QA + A^{\mathrm{T}} Q + C^{\mathrm{T}} C = 0.$$

(2) Compute an orthogonal real matrix V_A and V_D to put PQ into the Schur form

$$V_A^{\mathrm{T}} PQ V_A = \begin{bmatrix} \lambda_{A_{2m}} & * & \cdots & * \\ 0 & \lambda_{A_{2m-1}} & * & \vdots \\ \vdots & 0 & \ddots & * \\ 0 & \cdots & 0 & \lambda_{A_1} \end{bmatrix}, \quad V_D^{\mathrm{T}} PQ V_D = \begin{bmatrix} \lambda_{D_1} & * & \cdots & * \\ 0 & \lambda_{D_2} & * & \vdots \\ \vdots & 0 & \ddots & * \\ 0 & \cdots & 0 & \lambda_{D_{2m}} \end{bmatrix},$$

where $\{\lambda_{A_1} | i = 1, \ldots, k\} = \{\lambda_{D_1} | i = 1, \ldots, k\}$, $\{\lambda_{A_1} | i = k+1, \ldots, 2m\} = \{\lambda_{D_1} | i = k+1, \ldots, 2m\}$.

(3) Partition V_A and V_D as follows:

$$V_A = \left[\overbrace{V_{R,SMALL}}^{2m-k} \middle| \overbrace{V_{L,BIG}}^{k} \right], \quad V_D = \left[\overbrace{V_{R,BIG}}^{k} \middle| \overbrace{V_{L,SMALL}}^{2m-k} \right].$$

(4) Compute the singular-value decomposition for $V_{L,BIG}^{\mathrm{T}} V_{R,BIG}$ so that

$$V_{L,BIG}^{\mathrm{T}} V_{R,BIG} = U_{E,BIG} \sum_{E,BIG} V_{E,BIG}^{\mathrm{T}}.$$

(5) Compute the state-space realization of the final reduced order model $\tilde{G}(s)$,

$$\hat{A} = S_{L,BIG}^{\mathrm{T}} A S_{R,BIG}, \quad \hat{B} = S_{L,BIG}^{\mathrm{T}} B, \quad \hat{C} = C S_{R,BIG}, \quad \hat{D} = D, \tag{30}$$

where $S_{L,BIG} = V_{L,BIG} U_{E,BIG} \sum_{E,BIG}^{-1/2}$, $S_{R,BIG} = V_{R,BIG} V_{E,BIG} \sum_{E,BIG}^{-1/2}$.

The error bound is $\|G(s) - \hat{G}(s)\|_\infty \leqslant 2 \left(\sum_{i=k+1}^{n} \sigma_i \right)$.

4. DESIGN CONTROLLER BY LQG

For the final reduced order model $(\hat{A}, \hat{B}, \hat{C}, \hat{D})$, the LQG controller [13] is

$$\dot{\hat{x}} = [\hat{A} - \hat{B}K - L\hat{C} + L\hat{D}K]\hat{x} + Ly, \quad \hat{u} = K\hat{x}, \tag{31}$$

where $K = R^{-1} \hat{B}^{\mathrm{T}} P$, $L = P_0 \hat{C}^{\mathrm{T}} R_0^{-1}$, P and P_0 can be solved from the following two Riccati equations:

$$\hat{A}^{\mathrm{T}} P + P\hat{A} - P\hat{B} R^{-1} \hat{B}^{\mathrm{T}} P + Q = 0, \quad \hat{A}^{\mathrm{T}} P_0 + P_0 \hat{A} - P_0 \hat{C}^{\mathrm{T}} R_0^{-1} C P_0 + F Q_0 F^{\mathrm{T}} = 0, \tag{32}$$

where P denotes the semi-positive-definite weighting matrices on the states, Q the positive-definite weighting matrices on the control inputs, P_0 and Q_0 are the input noise intensity and measurement noise intensity, vector F denotes the disturbance position, y is the measurable output of the system $(\hat{A}, \hat{B}, \hat{C}, \hat{D})$.

5. NUMERICAL EXAMPLE

The methods outlined here are tested on the cantilever beam in Figure 1, whose dimensions are given in Table 1. The beam consists of an aluminum base beam with a layer

TABLE 1

System parameters

L	0·2616 m	h_b	0·002286 m	E_b	$7{\cdot}1 \times 10^{10}$ N/m^2	$\hat{\omega}$	10 000 rad/s
LL	0·027 m	h_v	0·00025 m	E_c	$7{\cdot}4 \times 10^{10}$ N/m^2	$\hat{\xi}$	4·0
LR	0·133 m	ρ_c	7600 kg/m^3	d_{31}	$-1{\cdot}75 \times 10^{-10}$ m/V		
b	0·0127 m	ρ_v	1250 kg/m^3	G^{∞}	5×10^5 Pa		
h_c	0·000762 m	ρ_b	2700 kg/m^3	α	6·0		

TABLE 2

Results of FEM analysis

	Mode 1	Mode 2	Mode 3	Mode 4
ACLD element numbers	Frequencies (Hz) (damping ratios)	Frequencies (Hz) (damping ratios)	Frequencies (Hz) (damping ratios)	Frequencies (Hz) (damping ratios)
2 ACLD elements	27·90 (2·56%)	150·12 (2·86%)	442·97 (3·15%)	831·76 (0·94%)
3 ACLD elements	27·90 (2·53%)	150·08 (2·82%)	441·77 (3·02%)	826·21 (1·03%)
4 ACLD elements	27·90 (2·52%)	150·06 (2·79%)	441·44 (2·96%)	825·13 (1·03%)
5 ACLD elements	27·87 (2·56%)	150·33 (2·75%)	442·02 (2·82%)	828·73 (0·94%)

of 3M ISD 112 VEM, followed by a PZT constraining layer. The beam is disturbed at the free tip of the cantilever beam; the transverse displacement response is measured there as well.

5.1. FEM ANALYSIS

In Figure 1, the left part of plain beam is divided into two plain beam elements; the right into three; and the middle into 2, 3, 4, 5 ACLD elements. Modal frequencies (Hz) and damping ratios of the first four modes are given in Table 2.

5.2. MODEL REDUCTION

In the last condition of Table 2, the system derived by FEM has 51 d.o.f.s in the physical space and 102 d.o.f.s in the state space. The system is unobservable and uncontrollable. It is necessary to perform model reduction and make the system observable and controllable before a controller is designed. Guided by section 3 and ACLD requirements, the transverse displacements of the 10 nodes and the axial displacements of the PZT layer of the six nodes in the ACLD elements are selected as master d.o.f.s. All dissipation co-ordinates, the system rotations and base beam axial displacements become slave d.o.f.s. Table 3 shows eigenvalues, modal frequencies and relative error of the first five modes for the full order model (FOM) and ROM in the physical space. Figure 3 is the ROM frequency response, derived by the methods described in section 3.1, compared with that of FOM. According to

TABLE 3

Eigenvalues, natural frequencies and damping ratios of the first five modes for the FOM and the ROM obtained by the methods described in section 3.1

Mode	Eigenvalue of FOM real part (imaginary part)	Eigenvalue of ROM real part (imaginary part)	Modal frequency of FOM (Hz)	Modal frequency of ROM (Hz)	Relative error of modal frequency (%)
1	− 2·2424	− 2·2425			
	(± 175·1236)	(± 175·1238)	27·87	27·87	0·000
2	−13·0059	−13·1036			
	(± 944·4660)	(± 944·6434)	150·33	150·36	0·01996
3	− 39·2062	− 39·60382			
	(± 2776·9938)	(± 2781·7158)	442·02	442·77	0·1696
4	− 24·3684	− 26·5048			
	(± 5207·0372)	(± 5233·4513)	828·73	832·94	0·5080
5	− 22·1051	− 23·6863			
	(± 8932·0711)	(± 9047·1374)	1421·59	1439·90	1·2880

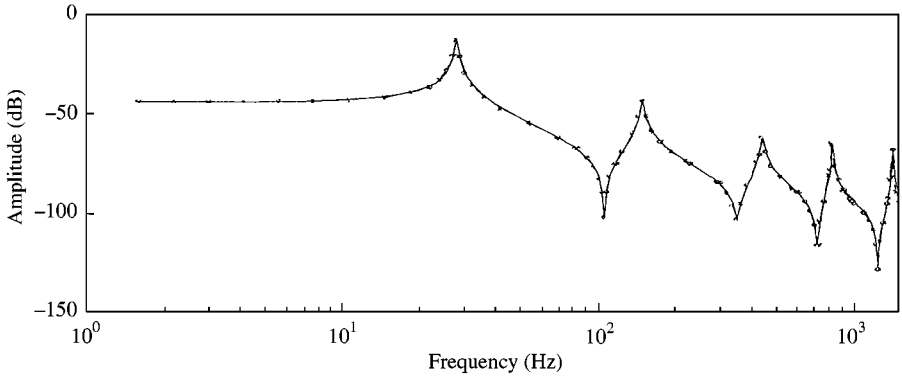

Figure 3. Comparison of the FRF for the FOM and the ROM obtained by the methods described in section 3.1: ——, full order model; – – –, reduced order model.

section 3, the condition of W_c and W_o is a good measure of controllability and observability. Table 4 is the condition of W_c and W_o of FOM and ROM.

From Table 3 and Figure 3, the following conclusions can be drawn: (1) The ROM obtained by the methods described in section 3.1 represents the FOM well in the low frequency range. (2) ROM approaches FOM from the upper bound. (3) Relative error increases when frequency increases. Table 4 shows that ROM and FOM are uncontrollable and unobservable according to section 3.

However, the design of a suitable controller depends on controllability and observability of the system. Robust model reduction (section 3.2) reduces the model from 32×32 to 6×6 in the state space. Table 5 gives eigenvalues, modal frequencies and relative error of the first three modes for the FOM and FROM in the state space. Figure 4 shows FROM frequency response derived by the methods described in section 3.2, compared with that of FOM. Figure 5 is the transverse displacement response at the free tip under the impulse disturbance. Table 6 is the condition of W_c and W_o of FOM and FROM.

Similarly, from Table 5, and Figures 4 and 5, the following conclusions can be drawn: (1) The FROM obtained by the methods described in section 3.2 represent the FOM well in the

TABLE 4

The condition of W_c and W_o of the FOM and the ROM obtained by the methods described in section 3.1

	Size (W_c)	Rank (W_c)	Rank (W_o)	Rank (W_o)
FOM	102	20	102	8
ROM	32	18	32	16

TABLE 5

The eigenvalues, natural frequencies and damping ratios of the first 3 *modes for the FOM and the FROM obtained by the methods described in section* 3.2

Mode	Eigenvalue of FOM real part imaginary part	Eigenvalue of FROM real part imaginary part	Modal frequency of FOM (Hz)	Modal frequency of FROM (Hz)	Relative error of modal frequency (%)
1	− 2·2424 (± 175·1236)	− 2·2022 (± 175·2783)	27·87	27·90	0·1076
2	−13·0059 (± 944·4660)	−13·1178 (± 948·8563)	150·33	151·03	0·4656
3	− 39·2062 (± 2776·9938)	− 41·9985 (± 2798·5747)	442·02	445·46	0·7782

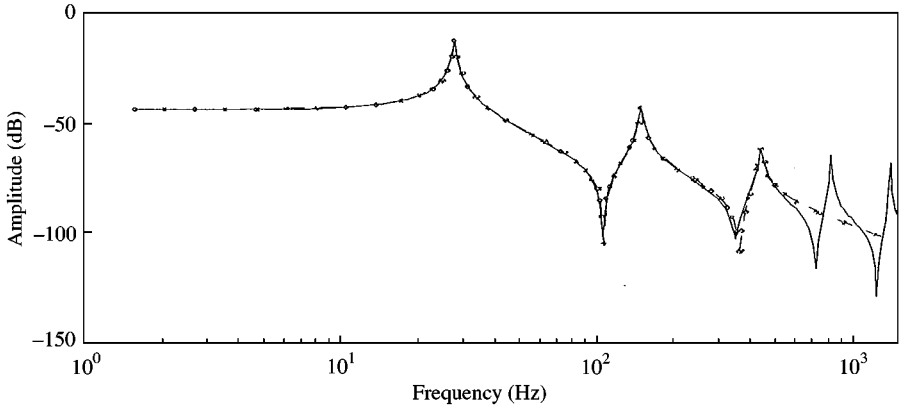

Figure 4. Comparison of the FRF for FOM and the FROM obtained by the method described in section 3.2: ——, full order model; – – –, final reduced order model.

low frequency range. (2) FROM approaches FOM from the upper bound. (3) Relative error increases as frequency increases. Table 6 shows that FROM is far smaller than FOM. Furthermore, FROM is controllable and observable, according to section 3.

5.3. DESIGN CONTROLLER BY LQG

The controllable and observable FROM obtained in section 5.2 accurately represents the FOM of the ACLD system. A FROM-based controller is designed accordingly as

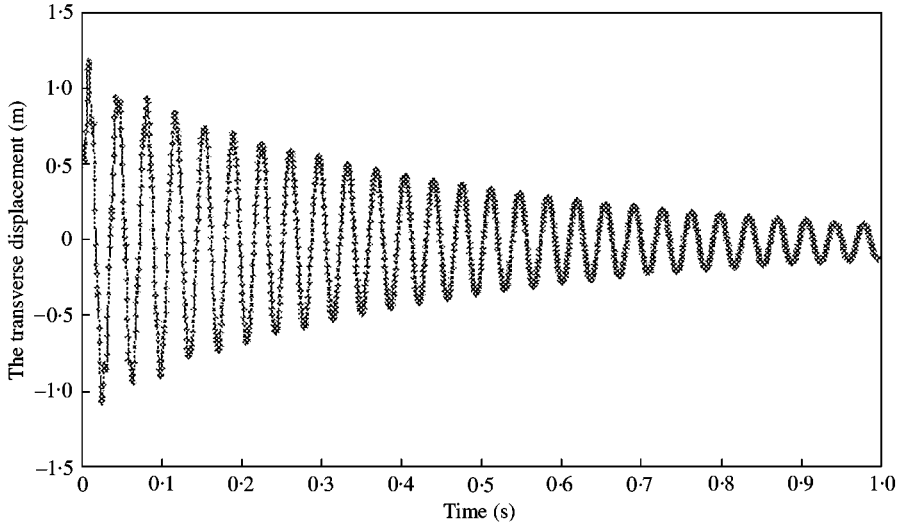

Figure 5. The transverse displacement response at the free tip under the impulse disturbance of the FOM and FROM: ——, full order model; – – –, final reduced order model.

TABLE 6

The condition of W_c and W_o of the FOM and the FROM obtained by the methods described in section 3.2

	Size (W_c)	Rank (W_c)	Rank (W_o)	Rank (W_o)
FOM	102	20	102	8
FROM	6	6	6	6

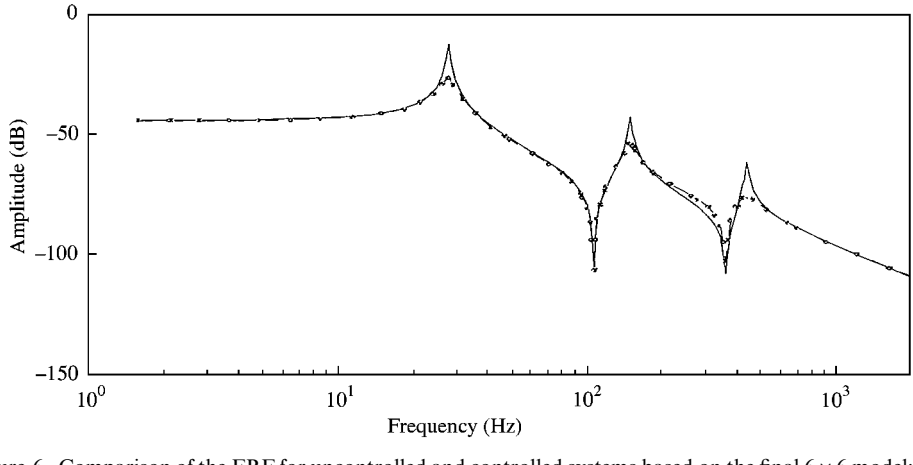

Figure 6. Comparison of the FRF for uncontrolled and controlled systems based on the final 6×6 model: ——, uncontrolled; – – –, controlled.

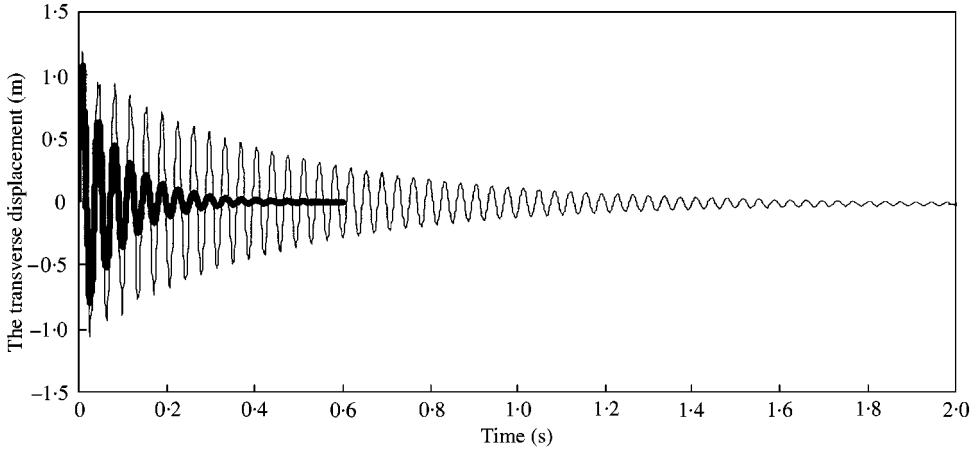

Figure 7. The transverse displacement response measured at the free tip of the cantilever beam with ACLD treatments under the impulse disturbance: ——, uncontrolled; ——, controlled.

mentioned in section 4. Weighting matrices Q and R are $5\times10^5\times\mathbf{I}$ and 1×10^{-4} respectively, I is the unit matrix with suitable size. Input noise intensity Q_0 and measurement noise intensity R_0 are 1×10^{-2} and 1×10^{-10} respectively. The cantilever beam's free tip is distributed. Output is the transverse displacement response measured there as well. The control force is the product of the voltage on the PZT. Figure 6 compares the FRF for uncontrolled and controlled systems. Figure 7 is the transverse displacement response measured at the free tip under the impulse disturbance. In Figures 6 and 7 vibration control is obvious.

6. CONCLUSION

A dynamic equation is derived by combining the FEM with the GHM model of VEM. A new procedure is proposed for reducing the model and making the FROM observable and controllable. A LQG controller is designed based on the final observable and controllable reduced order model. A numerical example proves that the model reduction procedure is effective and the vibration control is obvious.

REFERENCES

1. B. C. NAKRA 1984 *Shock and Vibration Digest* **16**, 17–22. Vibration control with viscoelastic material III.
2. A. K. LALL, N. T. ASNANI and B. C. NAKRA 1988 *Journal of Sound and Vibration* **123**, 247–259. Damping analysis of partially covered sandwich beams.
3. A. BHIMARADDI 1995 *Journal of Sound and Vibration* **179**, 591–602. Sandwich beam theory and the analysis of constrained layer damping.
4. F. E. CRAWLY and J. D. LUIS 1987 *American Institute of Aeronautics and Astronautics Journal* **25**, 1373–1385. Use of piezoelectric actuators as element of intelligent structures.
5. T. BAILY and J. E. HUBBARD 1985 *Journal of Guidance, Control and Dynamics* **8**, 605–611. Hubbard distributed piezoelectric polymer active vibration control of a cantilever beam.
6. S. S. RAO and T. S. PAN 1991 *American Institute of Aeronautics and Astronautics Journal* **29**, 442–443. Pan optimal placement of actuators in actively controlled structures using genetic algorithms.

7. A. BAZ and J. RO 1996 *Sound and Vibration* **3**, 18–21. The concept and performance of active constrained layer damping treatments.
8. S. SHIMAMURA 1984 *Bulletin of the Japan Institute of Metal* **23**, 656–661. A concept of intelligent materials.
9. D. F. GOLLA and P. C. HUGHES 1985 *Journal of Applied Mechanics* **52**, 897–906. Dynamics of viscoelastic structures—a time domain, finite element formulation.
10. D. J. MCTAVISH and P. C. HUGHES 1993 *American Society of Mechanical Engineers Journal of Vibration and Acoustics* **115**, 103–133. Modeling of linear viscoelastic space structures.
11. D. J. MEAD and S. MARKUS 1969 *Journal of Sound and Vibration* **10**, 163–175. The forced vibration of a three-layer damped sandwich beam with arbitrary boundary conditions.
12. M. G. SAFONOV and C. Y. CHIANG 1989 *IEEE Transaction on Automatic Control* **34**, 687–695. A Schur method for balanced-truncation model reduction.
13. M. ATHANS 1971 *IEEE Transaction on Automatic Control* **AC-16**, 529–552. The role and use of the stochastic linear-quadratic-Gaussian problem in control system design.
14. K. H. YAE and D. J. INMAN 1993 *Journal of Dynamic Systems, Measurement, and Control* **115**, 708–711. Control-oriented order reduction of finite element model.
15. R. J. GUYAN 1965 *American Institute of Aeronautics and Astronautics Journal* **3**, 380. Reduction of stiffness and mass matrices.
16. M. PAZ 1983 *Journal of Structural Engineering* **109**, 2591–2599. Practical reduction of structural eigenproblems.
17. E. J. DAVISION 1996 *IEEE Transaction on Automatic Control* **AC-11**, 93–101. A method for simplifying linear dynamic systems.
18. Z. Q. QU 1998 *Journal of Sound and Vibration* **214**, 965–971. A multi-step method for matrices condensation of finite element methods.
19. R. LEVY 1971 *NASTRAN User Experiences*, NASA, 201–220. Guyan reduction solutions recycled for improved accuracy.
20. J. N. RAMSDEN and J. R. STOCKER 1969 *International Journal for Numerical Method in Engineering* **1**, 339–349. Mass condensation—a semi-automatic method for reducing the size of vibration problems.
21. B. DOWNS 1980 *American Society of Mechanical Engineers Journal of Mechanical Design* **102**, 412–416. Accurate reduction of stiffness and mass matrices for vibration analysis and a rationale for selecting master degrees of freedom.
22. V. N. SHAH and M. RAYMUND 1982 *International Journal for Numerical Method in Engineering* **18**, 89–98. Analytical selection of masters for the reduced eigenvalue problem.
23. L. E. SUAREZ and M. P. SINGH 1992 *American Institute of Aeronautics and Astronautics Journal* **30**, 1046–1054. Dynamical condensation method for structural eigenvalue analysis.

APPENDIX A: NOMENCLATURE

b	width of ACLD beam
D	electrical displacement
d_{31}	piezoelectric constant
$[D]$	damping matrix
$E_{c,b}$	Young's modulus of PZT layer and base beam respectively
E	electrical field
$[F]$	general force including the effect of external disturbances and PZT layer
$\{f_c^{(e)}\}$	general force of the PZT layer
$\{f_d^{(e)}\}$	general force of external disturbances
G^{∞}	equilibrium value of shear modulus
G_v	shear modulus of VEM in time domain
$h_{c,v,b}$	thickness of PZT layer, VEM layer and base beam respectively
$I_{c,b}$	moment of inertia of PZT layer and base beam respectively
$[K]$	stiffness matrix
L_e	length of ACLD elements
L	length of the ACLD part
LL	length of the left part of ACLD beam
LR	length of the right part of the ACLD beam
$[M]$	mass matrix

$N_{w,c,b,v,\gamma}$	shape function of the transverse displacement, the axial displacement of PZT layer, the axial displacement of base beam, the axial displacement of VEM layer, the shear strain of VEM layer respectively
S_{11}^{E}	elastic compliance constant
$s\bar{G}(s)$	complex modulus of VEM layer
$\{U^{(e)}\}$	local nodal displacement vector
$u_{c,b}$	axial displacement of PZT layer and base beam respectively
$V(t)$	applied voltage on PZT layer
w	transverse displacement
$\hat{Z}_k(s)$	dissipation co-ordination
$\alpha_k, \hat{\omega}_k, \hat{\zeta}_k$	positive constants of GHM model
γ	shear strain of VEM layer
ε	mechanical strain in the axial direction
ε'_{33}	dielectric constant
θ	rotational angle
$\rho_{c,v,b}$	density of PZT layer, VEM layer and base beam respectively
σ_i	Hankel singular-values of the system
τ	mechanical stress in the axial direction

Superscript

$'$	partial differentiation with respect to x

Subscripts

b	base beam
c	PZT constraining layer
i, j	elemental node i, j
m	master d.o.f.s
s	slave d.o.f.s
R	reduced order system
u	axial displacement
v	viscoelastic layer
w	transverse displacement
γ	shear strain of VEM layer